JOURNAL OF COLLOID AND INTERFACE SCIENCE 162, 331–339 (1994)

Evolution of a Liquid Drop in a Spinning Drop Tensiometer

HOWARD H. HU[1] AND DANIEL D. JOSEPH*

*Department of Mechanical Engineering and Applied Mechanics, University of Pennsylvania, Philadelphia, Pennsylvania 19104-6315; and * Department of Aerospace Engineering and Mechanics and Minnesota Supercomputer Institute, University of Minnesota, Minneapolis, Minnesota 55455*

Received April 27, 1993; accepted August 30, 1993

To obtain desired material properties, a blend of two mostly incompatible polymers is often used. The blend morphology developed during the mixing process of molten polymers is strongly influenced by interfacial tension between the polymers. A spinning drop tensiometer is commonly used to measure the interfacial tension between two polymeric liquids. In this study a numerical method is developed which simulates the evolution of a liquid drop in a spinning drop apparatus. The Navier–Stokes equations are solved with a finite element formulation. A mixed Lagrangian and Eulerian technique is used to deal with the moving interface. The computation domain is remeshed and the flow field is interpolated to avoid mesh entanglement as drop deforms. The simulation generates relaxation curves for the radius and the length of the drop. The numerical results show that the shear stress on the drop surface is quite important. A simple theory of relaxation is then formulated which takes account of the shear stress on the surface of the cylindrical drop. It is found that the exponent for the relaxation of the drop depends on the interfacial tension, the equilibrium radius of the drop, the viscosities of both fluids, and the geometric ratios of the length to the radius of the drop and of the radius of the container to the radius of the drop. © 1994 Academic Press, Inc.

INTRODUCTION

To obtain desired material properties, a blend of two mostly incompatible polymers is often used. The properties of the polymer blend are, to a large extent, determined by the morphology of the blend, i.e., the size and shape of the dispersed phase and its distribution. The blend morphology and its stability are strongly influenced by the interfacial tension between liquid phases, the viscosity, and the viscoelastic properties of the molten polymers, the total strain, the processing time, and temperature, etc. (11). The addition of appropriate compatibilizers (surfactants) reduces the interfacial tension and improves the adhesion between two polymers (12). The optimization process involves the synthesis of the compatibilizer and the evaluation of its effect on the final blend and often implies time consuming feedback cycles. This process could be simplified if a method to evaluate the transient effect of the compatibilizers on the interfacial tension of the polymer melts were available.

There are several methods for measuring the interfacial tension between polymers: for example, the pendent drop or the sessile drop method, the method of capillary break up of a liquid thread, and the spinning drop method. A recent review on these methods was presented by Joseph *et al.* (6). Because of the high viscosity of most commercial polymers, equilibrium profiles of the interface between polymers are obtained only after a long time and with the risk of thermal degradation of the polymers. Changes in interfacial tension with time could be due to the establishment of equilibrium, to the formation of degradation products, or, in the case of systems containing a compatibilizer, to the adsorption–desorption of the compatibilizer to the interface.

In the spinning drop method, a drop of the less dense polymer melt is put into another polymer melt of higher density contained in a horizontal tube. The tube is spun at a constant speed. For each speed of rotation, the drop attains an equilibrium shape which is determined by the balance between the interfacial tension and the pressure difference at the interface caused by the centrifugal force and the density difference of the polymer melts (10, 9). Elmendorp and De Vos (2) suggested that the time of measurement could be shortened by an extrapolation of the transient state or by a forced attainment of the equilibrium shape. This was achieved by spinning the tube for a short while at a higher speed than the speed used at the final measurement. Joseph *et al.* (7, 6) developed a dynamic method for the measurement of a spinning drop in which the evolution of the shape of the drop was recorded as the angular speed of the tube was suddenly increased or decreased. They measured the relaxation curves for the drop diameter and obtained upper and lower bounds for the values of interfacial tension for many polymeric systems. The dynamic relaxation of the drop depends on material and interfacial properties of the polymer melts. One should be able to extract these properties from the measurement of the relaxation of the drop. Hsu and Flumerfelt (4) and Joseph *et al.* (6) developed simplified theories for the evolution of the radius of the spinning drop. However, the theories lack agreement with experiments.

[1] To whom correspondence should be addressed.

0021-9797/94 $6.00

In this study, numerical and analytical methods are used to describe the response of the shape of a spinning drop as the angular speed of the tube is suddenly increased or decreased. The fluids in the drop and in the continuous phase are assumed to be Newtonian. The numerical method is based on a finite element formulation (5). The interfacial tension, curvature, and discontinuous pressure across the interface are all incorporated in the formulation. A modified pressure is introduced because the pressure in fluids of rigid rotation is intrinsically quadratic, while in numerical schemes it is assumed to be linear locally in each small element. The error due to this locally linear pressure profile may dominate the weak flow due to the slow deformation of the drop. In the numerical method, the governing equations are solved with a Galerkin finite element formulation. A mixed Lagrangian and Eulerian technique is used to deal with the moving interface. The computation domain is frequently remeshed and the flow field is interpolated between meshes at different times to avoid mesh entanglement as the drop deforms. The numerical simulation generates relaxation curves for the radius and the length of the drop. The relaxation of the drop radius is basically exponential decay. The numerical results show that the shear stress on the drop surface is quite important. A simple theory of relaxation is then formulated which takes account of the shear stress on the surface of the cylindrical drop. It is found that the exponent for the relaxation of the drop depends on the interfacial tension, the equilibrium radius of the drop, the viscosities of both fluids, and the geometric ratios of the length to the radius of the drop and of the radius of the container to the radius of the drop.

DESCRIPTION OF THE PROBLEM

A spinning drop device is a rotating container loaded with two immiscible fluids. The axis of the container is perpendicular to gravity. The speed of rotation is high enough so that gravity effects are negligible. The fluid inside the drop is less dense and will centrifuge to the center of the container as shown in Fig. 1. Rigid rotations of two immiscible fluids with gravity neglected are unconditionally stable when the light fluid is inside (8). The equilibrium shape of the drop is determined by the balance between the interfacial tension and the pressure difference at the interface caused by the centrifugal force and the density difference of the two fluids (10). The parameter

$$J = \frac{(\rho_2 - \rho_1)\omega^2 \bar{R}^3}{T} \qquad [1]$$

is very important, where $\bar{R}$ is the root mean square radius of the drop, T is the interfacial tension, ω is the angular velocity, and (ρ_1, ρ_2) are the densities of the fluids inside and outside the drop. When $J > 4$, the equilibrium shape

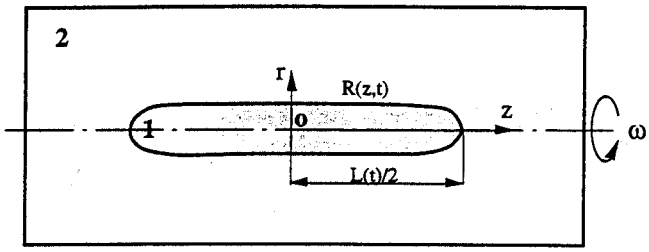

FIG. 1. Schematic of two fluids inside a rapidly rotating container. The less dense phase 1 stays at the center and is encapsulated by a denser continuous phase 2.

of the drop is a cylinder of constant radius $R = \bar{R}$. Actually, this solution can be realized only if there are end walls to restrain the expansion of the drop. If the drop is free to expand as ω increases, it will elongate indefinitely with the limit $J = 4$. When the ratio of length to diameter of the drop is $L/D \geqslant 4$, the value of the interfacial tension can be calculated from

$$T = \frac{(\rho_2 - \rho_1)\omega^2 D^3}{32}, \qquad [2]$$

where D is the measured maximum diameter of the equilibrium drop.

Assume that the spinning drop is initially at equilibrium, rotating rigidly with the container. Suddenly the angular velocity of the container is changed from ω_1 to ω_2. We wish to find out the motion of the fluids both inside and outside the drop and especially the evolution of the shape of the drop thereafter. Assume that the fluids are incompressible and Newtonian. The velocity $\mathbf{u}(\mathbf{x}, t)$ and the pressure $p(\mathbf{x}, t)$ both inside and outside the drop are governed by the Navier–Stokes equations

$$\nabla \cdot \mathbf{u} = 0,$$
$$\rho_i\left(\frac{\partial \mathbf{u}}{\partial t} + \mathbf{u} \cdot \nabla \mathbf{u}\right) = \nabla \cdot \sigma, \qquad [3]$$

where σ is the stress tensor given by

$$\sigma = -p\mathbf{1} + \mu_i[\nabla \mathbf{u} + (\nabla \mathbf{u})^{\mathrm{T}}], \qquad [4]$$

and ρ_i and μ_i ($i = 1$ and 2) are the densities and viscosities of fluids inside ($i = 1$) and outside ($i = 2$) the drop. Here the cylindrical coordinates (r, z, θ) are used, and the components of the velocity are (u_r, u_z, u_θ). Since the flow is axisymmetric ($\partial/\partial\theta = 0$), we need to look only at the (r, z) plane. The computation domain can be further reduced by half assuming that the drop is placed in the middle of the container (see Fig. 1).

The boundary conditions for the problem are the no-slip condition on the container walls, the centerline conditions

at the origin, $r = 0$, and the symmetry conditions at line $z = 0$.

The kinematic conditions at the interface are automatically satisfied because the domains, inside and outside the drop, share the common nodes at this interface. The dynamic conditions at the interface can be expressed as

$$[\sigma]\mathbf{n} = -T\kappa\mathbf{n}, \qquad [5]$$

where $[\sigma] = \sigma_1 - \sigma_2$ is the jump of stress tensor across the interface, $\mathbf{n}$ is the unit normal vector at the interface pointing outside the drop, and κ is the curvature of the interface whose value is positive for the drop shape shown in Fig. 1. Condition [5] simply means that the shear stresses are continuous across the interface and the difference in normal stress is balanced by the curvature of the interface and the interfacial tension between two fluids.

As the angular velocity of the container is suddenly changed, the rotational motion of very viscous fluids has two time scales. One is the viscous diffusion time required for the angular velocity of the fluids to adjust to the new value. The other is the evolution time of the drop. In our problem, the viscous diffusion time is much shorter than the evolution time of the drop. Thus the fluids in the container can be considered initially as fully spun-up:

$$u_r(\mathbf{x}, 0) = u_z(\mathbf{x}, 0) = 0 \quad \text{and} \quad u_\theta(\mathbf{x}, 0) = \omega_2 r. \qquad [6]$$

For rigid rotation of fluids, the pressure profile is quadratic in the radial direction:

$$p = \frac{\rho_i}{2}\omega^2 r^2 + \text{const.} \qquad [7]$$

However, in our discretization scheme, a linear profile of the pressure is assumed in each small element. This local linear pressure profile assumption produces an error which may dominate the weak flow during the slow evolution of the drop. Therefore a modified pressure is introduced to separate the quadratic part of the pressure:

$$p' = p - \frac{\rho_i}{2}\omega^2 r^2. \qquad [8]$$

The governing equations and the interfacial conditions are thus modified correspondingly. The pressures mentioned below all refer to this modified pressure.

NUMERICAL SCHEME

The numerical scheme we used involves three steps; see Hu *et al.* (5). The first step is automatic mesh generation according to the position of the interface. The second is projection of the flow field from one mesh onto another. The final step is the discretization and iterative solution of the Navier–Stokes equations.

Assume that at the current time instant t_{n+1}, based on the solution at a previous time, we are able to predict the new position of the interface. We then generate a new mesh on which we can discretize the Navier–Stokes equations and solve the flow field. We use unstructured meshes in which there is no one-to-one correspondence between the nodes of two meshes at two different times, which enables us to handle problems with large deformation. The mesh was generated by a variant of the Delaunay–Voronoi technique (3). Triangular P2/P1 elements are used in our finite element Navier–Stokes solver. In this element, the profiles of the three velocity components are assumed to be quadratic and the profile of the pressure is assumed to be linear. The generated elements are reordered to minimize the front-width in the solver. Some typical meshes used in the computation are displayed in Fig. 2.

After generating a new mesh which is not related to the old one, we need to interpolate the velocity field from the old mesh onto the new mesh in order to evaluate the time derivative term in the Navier–Stokes equations with the position $\mathbf{x}$ fixed:

$$\frac{\partial \mathbf{u}}{\partial t}(\mathbf{x}, t_{n+1}) = \frac{\mathbf{u}(\mathbf{x}, t_{n+1}) - \mathbf{u}(\mathbf{x}, t_n)}{t_{n+1} - t_n} + O(t_{n+1} - t_n).$$

More precisely, assume that we have a new mesh with nodes at $\mathbf{x}(t_{n+1})$ and that we have already calculated $\mathbf{u}(\mathbf{x}(t_n), t_n)$, the values of velocity at the mesh nodes $\mathbf{x}(t_n)$ of the previous time t_n. We want to project this velocity field onto the new mesh nodes $\mathbf{x}(t_{n+1})$ to get $\mathbf{u}(\mathbf{x}(t_{n+1}), t_n)$. In our projection routine, for each node $\mathbf{x}$ in the new mesh (at present time), we initiate a search in the old mesh (at previous time) to locate the element where the node $\mathbf{x}$ lies. Then inside that element the local coordinates for this node $\mathbf{x}$ are calculated.

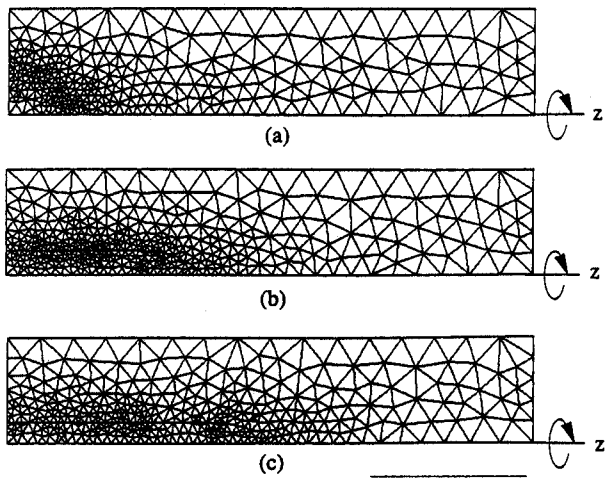

FIG. 2. Examples of meshes used in computation.

Finally the values of the components of velocity and acceleration are interpolated using their known values at the local nodes and the interpolation functions. However, some nodes that lie inside the drop in one mesh are found outside the drop in the other mesh, or vice versa. For these nodes, a Lagrangian scheme is introduced to evaluate their time derivatives. The nodes are traced back to find the approximate locations, $\mathbf{x}_0$, at the previous time, assuming that they move together with the interface. Then the values of the velocity at these locations, $\mathbf{x}_0$, are interpolated. The time derivative for these nodes is then expanded in a Taylor series around $t = t_n$ and $\mathbf{x} = \mathbf{x}_0$. The mixed Lagrangian–Eulerian scheme can be expressed as

$$\frac{\partial \mathbf{u}}{\partial t}(\mathbf{x}, t_{n+1}) = \frac{1+\beta}{\Delta t}[\mathbf{u}(\mathbf{x}, t_{n+1}) - \mathbf{u}(\mathbf{x}_0, t_n)] - \beta\left[\frac{\partial \mathbf{u}}{\partial t}(\mathbf{x}_0, t_n) + \mathbf{u}_m \cdot \nabla \mathbf{u}(\mathbf{x}_0, t_n)\right] - \mathbf{u}_m \cdot \nabla \mathbf{u}(\mathbf{x}, t_{n+1}) + O(\Delta t^{1+\beta}), \quad [9]$$

where

$$\mathbf{u}_m = (\mathbf{x} - \mathbf{x}_0)/\Delta t \quad [10]$$

is the mesh velocity and $\Delta t = t_{n+1} - t_n$. When $\beta = 0$, the scheme is first order, and when $\beta = 1$, the scheme is second order.

The Navier–Stokes solver used in our calculation is based on a finite element package, POLYFLOW; see Crochet *et al.* (1). The Navier–Stokes equations are solved with velocity and pressure as variables. They are discretized with a Galerkin finite element formulation in space and with a fully implicit finite difference scheme in time. At each time step, the resulting nonlinear matrix equations are handled by modified Newton iterations, and the linear equations in the iterations are solved by a frontal method.

In the Galerkin finite element formulation the solution and the variational function spaces for the pressure should include the functions which are discontinuous across the interface, because the pressure is discontinuous across the interface if the interfacial tension is not zero. Although the acceleration $d\mathbf{u}/dt$ of the interfacial nodes is continuous across the interface, the partial time derivative of the velocity $\partial \mathbf{u}/\partial t$ is discontinuous across the interface due to the motion of the interfacial nodes. These discontinuities are handled by introducing double values of pressure and time derivative of the velocity at the interfacial nodes, which introduces some level of difficulties in programming.

The scheme used in this study is described below.

(1) Initialization: Set $t_0 = 0$ and $n = 0$ (index for time step); initialize velocity field and positions of the interfacial nodes.

(2) Predict: Select an appropriate time step Δt_{n+1} with $t_{n+1} = t_n + \Delta t_{n+1}$; set $k = 0$ (iteration counter); predict the new locations of the interfacial nodes $\mathbf{x}_i(t_{n+1}) = \mathbf{x}_i(t_n) + \Delta t_{n+1}\mathbf{u}_i(t_n) + (\Delta t_{n+1}^2/2)\mathbf{a}_i(t_n)$, where $\mathbf{x}_i$, $\mathbf{u}_i$, and $\mathbf{a}_i$ are the position, velocity, and acceleration of the interfacial nodes.

(3) Remeshing and Projection: Generate a new mesh $\mathbf{x}(t_{n+1})$; interpolate the velocity field $\mathbf{u}(\mathbf{x}(t_{n+1}), t_n)$ from $\mathbf{u}(\mathbf{x}(t_n), t_n)$ and evaluate the time derivatives using [9].

(4) One-Step Navier–Stokes Iteration: on the new mesh $\mathbf{x}(t_{n+1})$ with $\mathbf{u}(\mathbf{x}(t_{n+1}), t_n)$ as initial values, perform *one* Newton iteration in the Navier–Stokes solver to get a flow field $\mathbf{u}^{(k)}(\mathbf{x}(t_{n+1}), t_{n+1})$ and $p^{(k)}(\mathbf{x}(t_{n+1}), t_{n+1})$; retrieve the velocity on the interfacial nodes $\mathbf{u}_i(t_{n+1})$.

(5) Update: $k \Leftarrow k + 1$; the predicted position of the interfacial nodes is updated and the mesh is modified $\mathbf{x}_i(t_{n+1}) = \mathbf{x}_i(t_n) + (\Delta t_{n+1}/2)[\mathbf{u}_i(t_n) + \mathbf{u}_i(t_{n+1})]$.

(6) Convergence Test: $\epsilon = \|\mathbf{u}^{(k)}(\mathbf{x}(t_{n+1}), t_{n+1}) - \mathbf{u}^{(k-1)}(\mathbf{x}(t_{n+1}), t_{n+1})\|$. If ϵ is larger than a prescribed value go to step (4), otherwise $\mathbf{u}(\mathbf{x}(t_{n+1}), t_{n+1}) = \mathbf{u}^{(k)}(\mathbf{x}(t_{n+1}), t_{n+1})$, $p(\mathbf{x}(t_{n+1}), t_{n+1}) = p^{(k)}(\mathbf{x}(t_{n+1}), t_{n+1})$.

(7) If the time t_{n+1} is less than T then reset $n \Leftarrow n + 1$ and go to the next time step (2); otherwise stop.

The scheme is fully implicit. Even the position of the interface is determine implicitly at each time step by means of iteration as shown in step (5). The time accuracy of the scheme is Δt^2. The time step Δt_{n+1} in the scheme is chosen to restrict the maximum distance each interfacial node can move in one step. The Jacobian matrix for the linearized equations in the nonlinear Newton iteration of the Navier–Stokes solver is calculated and inverted once, and is recalculated and inverted only when the rate of convergence of the iteration is too slow.

NUMERICAL RESULTS

In our numerical simulation we fixed the size of the container; its radius is 1 cm and its length is 10 cm. In the first example, the viscosities and densities of the fluids inside and outside the drop are (1000 poise, 1.0 g/cm^3) and (14.1 poise, 1.26 g/cm^3), respectively. The interfacial tension between the two fluids is 20 dyn/cm. The angular velocity of the container is increased from 0 to 2000 rpm. The initial shape of the drop is a sphere of radius 0.5 cm. According to [2], the equilibrium radius of the drop should be $R_{eq} = 0.1914$ cm. Figure 3 shows the shape of the drop as it evolves from a spherical shape to a long cylindrical one.

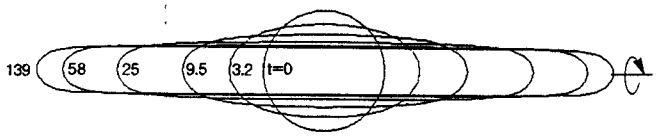

FIG. 3. Evolution of a spinning drop from the initial spherical shape to a long cylindrical shape.

Figure 4a plots the relaxation curves for the radius and the length of the drop which spins under the same conditions as described above. The numerical asymptotic value of the radius of the drop is the same as the exact value calculated from [2]. The relaxation curve for the radius of the drop is fitted into an exponential function of the form

$$R_{eq} + a \cdot e^{-mt}, \qquad [11]$$

where R_{eq} is the equilibrium value (when $t \to \infty$) of the radius, $R_{eq} + a$ is the initial radius, and m is the exponent representing the rate of decay. In Fig. 4b, we present the curve fit for the radius of the drop. A constant exponent fits the relaxation curve satisfactorily, except at the early times when the drop relaxes faster. Also presented in Fig. 4b is the approximation to the volume of the drop $\sim \pi R^2 L$. The nearly constant value of the approximation can be used to relate the relaxation curves for the radius and for the length of the drop.

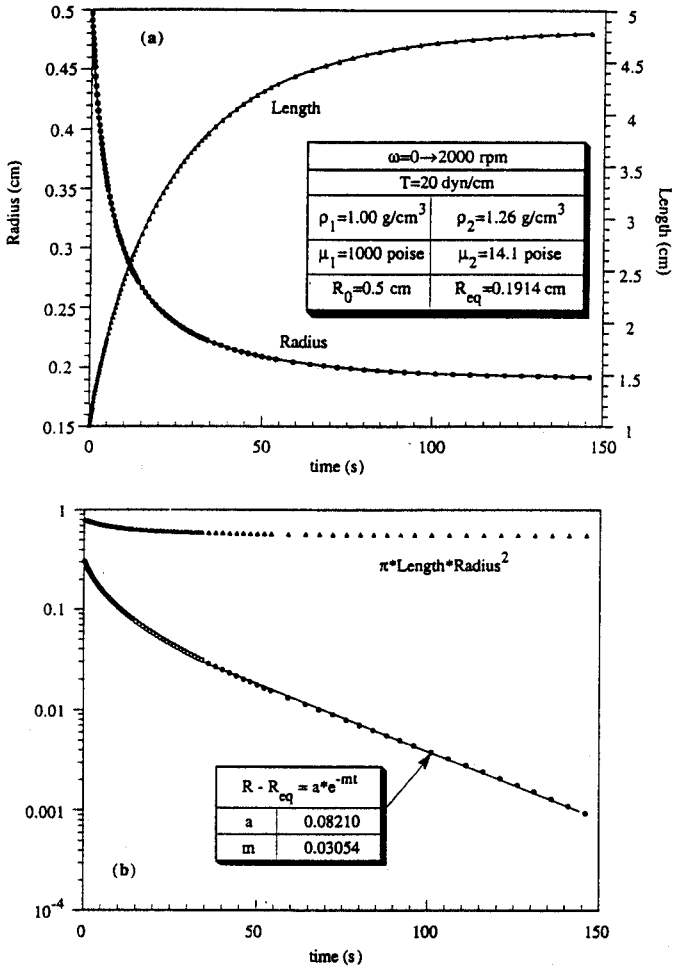

FIG. 4. Relaxation curves for the radius and the length of a spinning drop. The fluids are spun up from 0 to 2000 rpm.

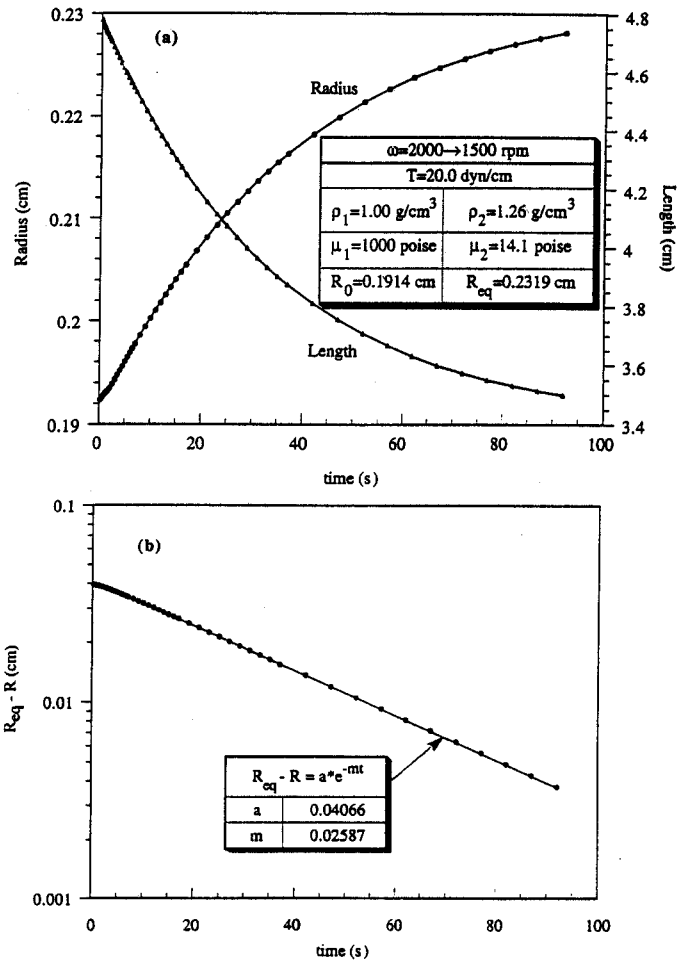

FIG. 5. Relaxation curves for the radius and the length of a spinning drop. The fluids are spun down from 2000 to 1500 rpm.

When the drop reaches equilibrium at 2000 rpm, the angular velocity of the container is reduced to 1500 rpm. Figure 5 presents the relaxation curves and the exponential fit. In this spindown test, the exponential function fits well for the whole time interval. The exponent in this case is different from the ones found in Fig. 4. Next, from 1500 rpm the drop is spun up to 2000 rpm, as shown in Fig. 6. The exponent is very close to the value obtained in Fig. 4. More tests show that the relaxation of the drop depends on the final equilibrium state of the drop, not the initial shape of the drop.

Some of the meshes used in the computation of Fig. 4 are displayed in Fig. 2. They are quite refined. A convergence test was performed on a coarser mesh which basically gives the identical relaxation curves. Another test was run by doubling the time step used above; there is no noticeable change in the relaxation curves. Thus our numerical results are converged and accurate.

Using the spin-up from 1500 rpm to 2000 rpm as a standard procedure, we test the effects of different combinations

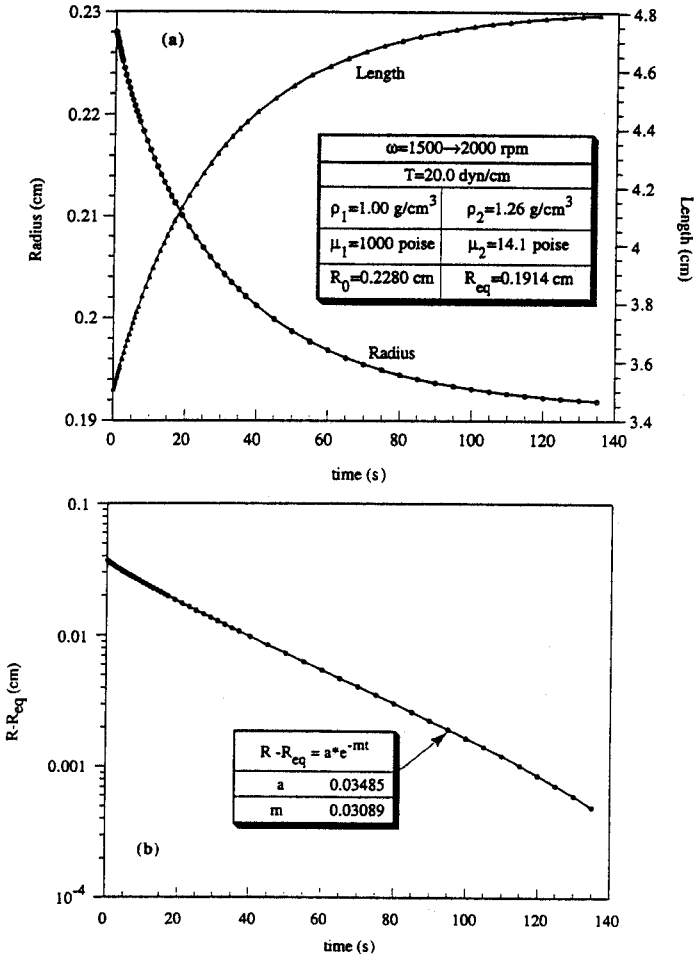

FIG. 6. Relaxation curves for the radius and the length of a spinning drop. The fluids are spun up again from 1500 to 2000 rpm.

of the material properties. For each case the exponent is calculated and the results are listed in Table 1. By examining the parameters and the values of the exponent m, we find the correlation

$$m = \frac{T}{\mu_1 R_{eq}} f\left(\frac{\mu_2}{\mu_1}\right), \qquad [12]$$

where

$$R_{eq}^3 = \frac{4T}{(\rho_2 - \rho_1)\omega^2} \quad \text{and}$$

$$f\left(\frac{\mu_2}{\mu_1}\right) = \frac{0.553}{1 + 63.4\mu_2/\mu_1}. \qquad [13]$$

Function f is fitted from the parameters listed in the table; see Fig. 7. Correlation [12] fits all of our data well.

TABLE 1
Exponent of Relaxation of a Spinning Drop When it is Spun up from 1500 to 2000 rpm

1	$(\rho_1, \mu_1) = (1.0, 1000)$, $(\rho_2, \mu_2) = (1.26, 14.1)$, and $T = 20$	$m = 0.0309$
2	$(\rho_1, \mu_1) = (1.0, 4000)$, $(\rho_2, \mu_2) = (1.26, 14.1)$, and $T = 20$	$m = 0.0117$
3	$(\rho_1, \mu_1) = (1.13, 1000)$, $(\rho_2, \mu_2) = (1.26, 14.1)$, and $T = 10$	$m = 0.0150$
4	$(\rho_1, \mu_1) = (1.0, 1000)$, $(\rho_2, \mu_2) = (1.26, 30)$, and $T = 20$	$m = 0.0198$
5	$(\rho_1, \mu_1) = (1.0, 8000)$, $(\rho_2, \mu_2) = (1.26, 14.1)$, and $T = 20$	$m = 0.00655$
6	$(\rho_1, \mu_1) = (1.0, 1000)$, $(\rho_2, \mu_2) = (1.26, 100)$, and $T = 20$	$m = 0.00861$

Note. The radius of the drop is fitted into a function of form $R = R_{eq} + a \cdot e^{-mt}$. The unit for the density is g/cm^3, the unit for the viscosity is poise, and the unit for the interfacial tension is dyn/cm.

A SIMPLIFIED THEORY

As mentioned above, for a pair of very viscous fluids in this spinning drop problem, the viscous diffusion time is much shorter than the evolution time of the drop. The fluids in the container can be considered initially as fully spun-up. The drop deforms because of an imbalance of the normal stress at the interface and the interfacial tension. One can think of this problem as the deformation of the drop under a squeeze at the surface of the drop. In an early analysis, Hsu and Flumerfelt (4) assumed that the flow inside and outside the drop was purely extensional, thus there was no shear on the surface of the drop. They derived an evolution equation for the radius of the drop. Recently Joseph *et al.* (6) modified Hsu and Flumerfelt's derivation by including the inertial terms and assuming the form of the curvature at the end tip of the drop. For Newtonian fluids close to equilibrium, Joseph *et al.* (6) derived that the relaxation exponent for the radius of the drop is

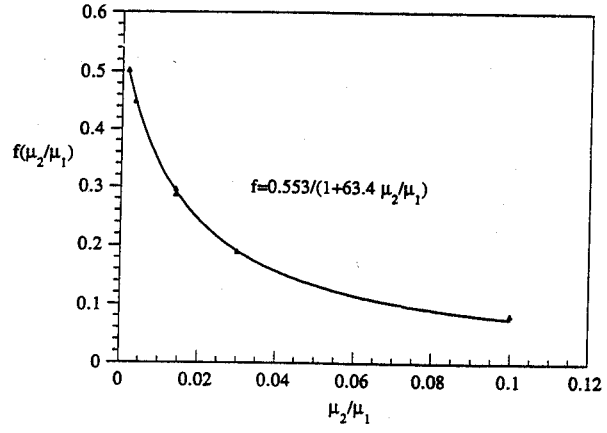

FIG. 7. Curve fit for the function f in the correlation of the relaxation exponent m.

$$m = \frac{T}{(\mu_1 - \mu_2)R_{eq}}. \qquad [14]$$

However, Eq. [14] lacks agreement with their experimental data. It usually gives a faster relaxation for the radius of the drop than that observed in the experiments, as noted by Joseph *et al.* (6). The exponent calculated from [12] is much smaller than that calculated from [14], indicating a slow relaxation which should give a much better agreement with the experiments. It is also noted from [12] that the relaxation of the drop radius slows down as the viscosities of the fluids, both inside and outside the drop, increase. This is more reasonable than the result concluded from [14] which states that the relaxation of the drop gets faster if the viscosity outside the drop increases.

Here, using the information from our numerical results, we examine the assumptions made in the derivation of Joseph *et al.* (6) and try to develop a simplified theory that would describe the evolution of the radius of the drop.

Figure 8 displays the streamlines at different times for flow inside and outside the drop. The shape of the drop and the flow conditions are the same as those presented in Figs. 3 and 4. Obviously the drop contracts in the radial direction and extends along its length. The iso-lines of the velocity components u_r and u_z are plotted in Fig. 9. The u_z lines clearly show that there is shear stress at the surface of the drop. We think that the shear stress on the surface of the drop is quite important and should be included in the simplified theory.

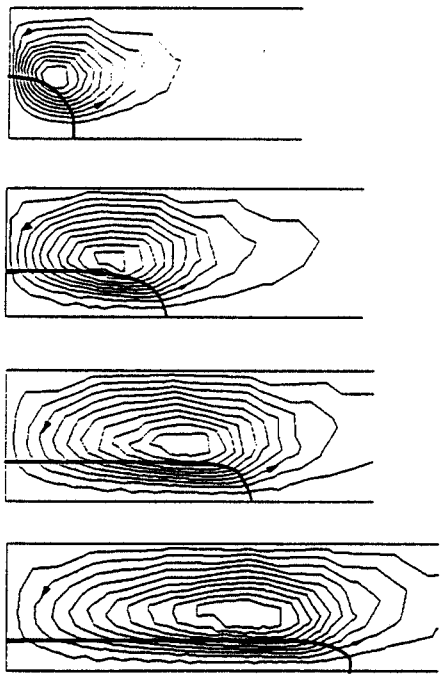

FIG. 8. Isostreamlines around the spinning drop.

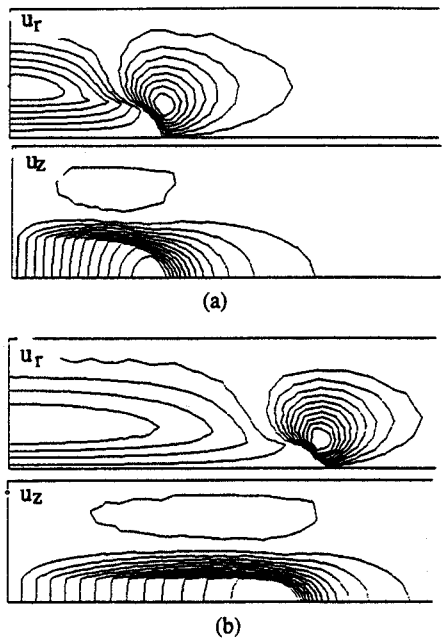

FIG. 9. Isovelocity lines inside and outside the spinning drop: (a) is at an early time and (b) is at a later time when the drop has almost reached equilibrium.

Joseph *et al.* (6), based on a quasi-steady argument, assumed that the total curvature at the end tip of the drop ($r = 0$, $z = L$) $2H_L$ can be expressed as

$$2H_L R = 3, \qquad [15]$$

where R is the time-dependent maximum radius of the drop. However, based on the numerical results, this curvature is better fitted by

$$H_L(R + R_{eq}) = 3, \qquad [16]$$

as indicated in Fig. 10.

Following the analysis of Joseph *et al.* (6), we make two modifications. One is to add a pressure gradient along the length of the drop due to the shear stress on the surface of the drop; the other is to use assumption [16] instead of [15]. The shear stress on the surface of the drop is estimated by

$$\tau = \mu_2 \frac{u_z}{R \ln(R_0/R)}, \qquad [17]$$

where R_0 is the inner radius of the tube and u_z is the extensional velocity of the surface of the drop. Equation [17] is derived by assuming that cylindrical drop is rigid, surrounded by the fluid outside, and moving inside a tube. By a balance of force on the drop as shown in Fig. 11, the pressure gradient due to the shear stress can be evaluated as

$$\frac{\partial p_i}{\partial z} = -\frac{2}{R}\tau. \qquad [18]$$

Then the two normal stress balance conditions, at the end tip of the drop ($r = 0$, $z = L/2$) and at the central surface of the drop ($r = R$, $z = 0$), yield the evolution equation

$$-\frac{\mu_1}{T}\left[3(1-\mu_2/\mu_1)+\frac{\mu_2/\mu_1}{4\ln(R_0/R)}\frac{L^2}{R^2}\right]\dot{R} - \left(\frac{R}{R_{eq}}\right)^3+\left(H_L R-\frac{1}{2}\right)=0 \quad [19]$$

for the radius of the drop, where $\dot{R}$ is the rate of change of the drop radius. Equation [19] can be linearized around the equilibrium state $R = R_{eq}$,

$$\frac{R_{eq}\mu_1}{T}\left[3+\left(\frac{L_{eq}^2/R_{eq}^2}{4\ln(R_0/R_{eq})}-3\right)\frac{\mu_2}{\mu_1}\right]\dot{\epsilon}+\frac{9}{4}\epsilon=0, \quad [20]$$

where $\epsilon = R/R_{eq} - 1$, and L_{eq} is the equilibrium length of the drop. From [20] the exponent for the relaxation curve can be easily found.

$$m=\frac{T}{\mu_1 R_{eq}}0.75\Big/\left(1+\left(\frac{L_{eq}^2/R_{eq}^2}{12\ln(R_0/R_{eq})}-1\right)\frac{\mu_2}{\mu_1}\right). \quad [21]$$

For the parameters used in our numerical simulation, the above exponent has an expression

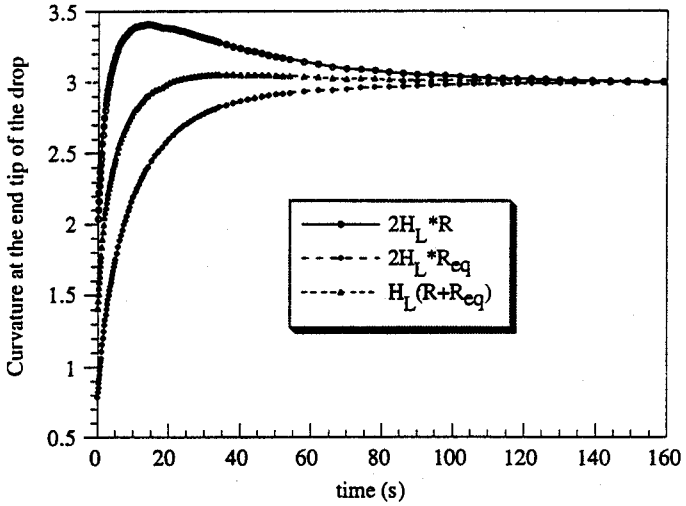

FIG. 10. Evolution of the total curvature at the end tip of the drop $2H_L$. The curve of $H_L(R + R_{eq}) = 3$ fits this curvature best for times later than 20 s.

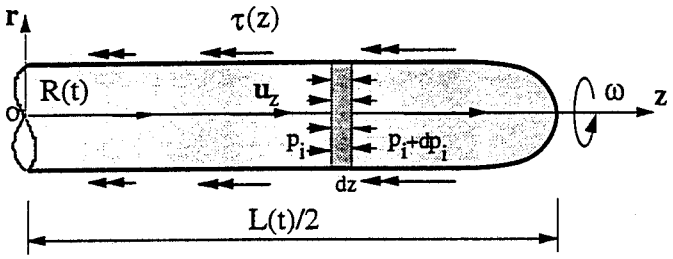

FIG. 11. Shear stress on the surface of the spinning drop.

$$m=\frac{T}{\mu_1 R_{eq}}\frac{0.75}{1+31.5\mu_2/\mu_1}, \quad [22]$$

which has the same form as [12]. However, the values of coefficient are different from our curve-fitted expression. The value predicated by [22] is larger than that predicated by [12], indicating the relaxation of the drop is still too fast. The detailed flow around the end caps of the drop would slow down the relaxation of the drop and account for this difference. Equation [21] indicates that the value of the exponent depends on the geometric ratios of the length to the radius of the drop and of the radius of the container to the radius of the drop, which is more complicated than we thought. Comparison of our prediction with the available experimental data is hard to make, because in all of the experiments performed only limited information was recorded.

CONCLUSIONS

The numerical simulation presents detailed information about the flow inside and outside the drop. It generates relaxation curves of the radius and length of the drop. These results show that the flow inside the drop is essentially extensional. The shear stress on the drop surface is quite important, which is neglected in the analysis by Joseph *et al.* (6). The relaxation of the drop radius is basically exponential decay. A simple theory of relaxation has been formulated based on the numerical simulation. This theory takes account of the shear stress on the cylindrical drop surface. It is found that the exponent of the relaxation of the drop depends on the interfacial tension, the equilibrium radius of the drop, the viscosities of both fluids, and the geometric ratios of the length to the radius of the drop and of the radius of the container to the radius of the drop. This theory agrees better with the experimental data than the one presented by Joseph *et al.* (6). Using this theory, transient measurements of the drop shape can be used to extract the rheological properties and the interfacial tension of the fluids.

ACKNOWLEDGMENTS

HHH acknowledges support from NSF DMR91-20668 through the Laboratory for Research on the Structure of Matter at the University of Pennsylvania and from the Research Foundation of the University of Pennsylvania. DDJ was supported by the Department of Energy, the National Science Foundation, the Hoechst-Celanese Corp., the Army Research Office, Mathematics, the Army High Performance Computing Research Center, and the Minnesota Supercomputer Institute.

REFERENCES

1. Crochet, M. J., Debaut, B., Keunings, R., and Marchal, J. M., *in* "CAE for Polymer Processing: Application in Extrusion and Other Continuous Processes" (K. T. O'Brian, Ed.), Hanser Verlag, Munich, 1991.
2. Elmendorp, J. J., and De Vos, G. *Polym. Eng. Sci.* **26,** 415 (1986).
3. Hecht, F., and Saltel, E., "Emc^2 un logiciel d'édition de maillages et de contours bidimensionels," Rapport, INRIA, 1989.
4. Hsu, J. C., and Flumerfelt, R. W., *Trans. Soc. Rheol.* **19,** 523 (1975).
5. Hu, H. H., Joseph, D. D., and Crochet, M. J., *Theor. Comput. Fluid Dyn.* **3,** 285 (1992).
6. Joseph, D. D., Arney, M., Gillberg, G., Hu, H. H., Hultman, D., Verdier, C., and Vinagre, H., *J. Rheol.* **36,** 621 (1992).
7. Joseph, D. D., Arney, M. S., and Ma, G., *J. Colloid Interface Sci.* **148,** 291 (1992).
8. Joseph, D. D., and Preziosi, L., *J. Fluid Mech.* **185,** 323 (1987).
9. Patterson, H. T., Hu, K. H., and Grindstaff, T. H., *J. Polymer Sci., Part C* **34,** 31 (1971).
10. Vonnegut, B., *Rev. Sci. Instrum.* **13,** 6 (1942).
11. Wu, S., *Polym. Eng. Sci.* **27,** 335 (1987).
12. Xanthos, M., *Polym. Eng. Sci.* **28,** 1392 (1988).